Searching for clock-type anisotropy in honeycomb antiferromagnet $CoTiO_3$

K. MacFarquharson[1]

[1]*Clarendon Laboratory, Department of Physics, University of Oxford, Parks Road, Oxford OX1 3PU, UK*

(Dated: August 25, 2020)

Recent models have suggested an unusual anisotropy in the antiferromagnetic phase of $CoTiO_3$. This 'clock' anisotropy has sixfold symmetry within an easy plane. In this report I lay out what the effects of such an anisotropy might be and try to identify key features that could demonstrate its existence. Then I describe experimental probes to identify these effects. Finally I present experimental results using magnetisation measurements and angular dependence of magnetic torque of $CoTiO_3$ as a function of temperature and field.

INTRODUCTION

Much of modern condensed matter physics involves itself with searching for interesting, non-trivial band structures. This is in part because many of the more recently predicted properties of crystals are caused directly by band structure[1] including topological insulators [2, 3], magic-angle graphene[4], and Weyl semi-metals [5]. Another area that can be explored is the magnon band structure in magnetic materials. In these too, a number of non-trivial topologies have been discovered or predicted [5–8].

The honeycomb quantum magnet $CoTiO_3$ is of particular interest because its layered honeycomb structure makes it a magnetic analogue of graphene. The discovery of graphene's massless Dirac electrons resulted in an explosion of publications[1, 9–11] and so there is much interest in other materials with Dirac points, or Dirac nodal lines. Recent neutron diffraction studies on $CoTiO_3$ have shown an rich complexity in magnon band structure [12, 13], including Dirac nodal lines which wind around the $\vec{c}$ axis. $CoTiO_3$ has stacked honeycomb layers (Fig 1) of magnetic Co^{2+} ions located in the centre of oxygen octahedra.

The neutron scattering experiments [12] suggest a Hamiltonian with bond-dependent anisotropic exchange interactions, resulting in a low energy spectral gap in magnon diffraction. This suggests the existence of an anisotropy in the orientation of ordered spins within the ab easy plane of the crystal. This would result in a weakly anisotropic magnetisation which can be explored with magnetometry techniques. This report seeks to explore the effects of such an anisotropy and how it might be detected experimentally.

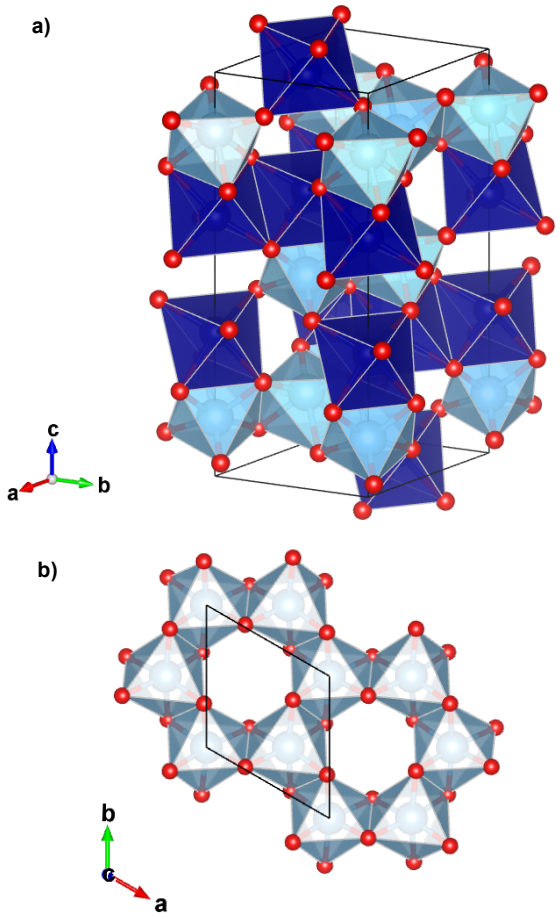

FIG. 1. Crystal Structure of $CoTiO_3$ rhombohedral unit cell ($R\bar{3}$). a) Schematic of the structural hexagonal unit cell (solid outline) showing TiO_6 and CoO_6 octahedra shaded in dark/light blue with oxygens as red balls. b) Honeycomb arrangement of cobalt ions in the ab plane.

MODEL

A minimal model proposed to capture the observed magnetic structure and key features of the dispersions in $CoTiO_3$ is [12]

$$\hat{\mathcal{H}}_H = \sum_{\langle i,j\rangle_n} J_n^{\perp}(S_i^x S_j^x + S_i^y S_j^y) + J_n^z S_i^z S_j^z \qquad (1)$$

where the sum is over pairs of spins $\langle i,j\rangle_n$ of the n'th nearest neighbours, with $J_{1,2,3}$ for intralayer bonds and $J_{2,4,6}$ for interlayer bonds. Here $S^{x,y,z}$ are components along a Cartesian frame ($\vec{x} \parallel \vec{a}, \vec{z} \parallel \vec{c}$) of the pseudo-spin $S = \frac{1}{2}$ that defines the ground state Kramers doublet of the Co^{2+} ions ($3d^7$) after including the effects of the octahedral trigonal crystal field and the spin-orbit coupling [12].

This is combined with a Zeeman term

$$\hat{\mathcal{H}}_Z = \sum_i \mu_B \vec{B}\,\bar{\bar{g}}\,\vec{S}_i \tag{2}$$

where the g-tensor has the uniaxial form

$$\bar{\bar{g}} = \mathrm{diag}(g_\perp, g_\perp, g_\parallel) \tag{3}$$

due to a 3-fold point group symmetry at the Co sites, with $g_\parallel$ along the $\vec{c}$ -axis.

The magnetic structure of $CoTiO_3$, as measured by neutron diffraction [14] has spins aligned ferromagnetically in layers in the ab plane. Adjacent layers are antiparallel due to antiferromagnetic couplings between layers. This is captured in Eq. (1) with the dominant intralayer ferromagnetic nearest-neighbour couplings ($J_1^\perp < 0$) and antiferromagnetic interlayer couplings. Eq. (1) is a simplification as it assumes no dependence on the orientation of the spins in the ab plane. This would manifest experimentally as a gapless Goldstone (magnon) mode associated with spin rotations in the ab plane. However, inelastic neutron scattering experiments [12] show a clear gap in this mode $\Delta \sim 1\,\mathrm{meV}$. This indicates an anisotropy within the ab plane. The total energy is expected to be invariant under all point group symmetry operations of the lattice ($\bar{3}$) and also under time reversal (reversing the orientations of all spins). Together this constrains the energy dependence of the spin orientations in the ab plane to have 6-fold symmetry. So a simple form is proposed

$$H_A(\theta) = E_A \cos 6(\theta - \theta_0) \tag{4}$$

where θ is the azimuth of the ordered spins in the ab plane relative to some reference direction, and E_A is an energy that controls the strength of the anisotropy. This anisotropy is called clock anisotropy because the easy (hard) axes fall on the even (odd) numbers of an analogue clock. Note that the energy is unchanged by a $180°$ rotation about the $\vec{c}$ axis so the same term is used for both sublattices in the antiferromagnetic structure. Considering just the locations of Co^{2+} ions in the ab plane, the lattice has $\bar{3}m$ symmetry with mirror planes containing the $\vec{c}$ axis. This would restrict θ_0 such that energy minima (maxima) occur when spins are aligned parallel to the Co-Co bond directions of the honeycomb layers for $E_A > 0$ ($E_A < 0$). However, a small distortion in the oxygen octahedra breaks this symmetry and lowers the symmetry to $\bar{3}$. Instead, a reference direction is chosen such that $\theta_0 = 0$, i.e. the reference direction is taken along the energy maxima. The proposed microscopic origin of the anisotropy term (eq. 4) is an anisotropic interaction between nearest neighbour spin components parallel to and perpendicular to bonds in the plane $\eta = J_1^{yy} - J_1^{xx}$ where x, y denote local directions parallel and perpendicular to the Co-Co bond directions respectively. This gives a ground state contribution of the form of Eq. (4) with $E_A \sim -\eta^3$ [12]. ‘ At the mean-field level,the solution of the Hamiltonian in equations (1) + (2) + (4) can be found by solving for the equilibrium orientation of the spins ($\vec{S_1}$, $\vec{S_2}$) of two types of layers (sublattices) of the AFM structure. So the resulting two-spin mean-field Hamiltonian becomes

$$\hat{\mathcal{H}} = J\vec{S_1}\cdot\vec{S_2} + \sum_i g\mu_B\vec{B}\cdot\vec{S_i} + \sum_i E_A\cos(6\theta_i) \tag{5}$$

where J parameterises the antiferromagnetic coupling of the two sublattices, $i \in \{1,2\}$ and $\vec{S_1}$, $\vec{S_2}$ are the vector spins of the two sublattices and $g = g_\perp$. The above equation assumes the field is applied within the ab plane and the spins are confined to this plane. This is the arrangement where the system is most sensitive to E_A and so is discussed here to identify key features. If the field had some component parallel to $\vec{c}$, the spins would cant out of the ab plane, and the anisotropy in $\hat{g}$ would need to be considered, as well as a term to prefer the spins aligned in-plane.

Considering the results of this much simplified, semi-classical model will enable me to identify experimental signatures of this anisotropy in real experiments. The angular-dependent energy term in Eq. (4) has been proposed to arise from an order-by-disorder [15–18] mechanism in a quantum treatment of the spin Hamiltonian including the XXZ form in Eq. (1))= as well as the bond dependent exchange η [12]. A direct experimental signature of this term would be strong evidence for the validity of this model.

CALCULATION OF BEHAVIOR OF CLOCK-ANISOTROPY SYSTEM

Treating the spins as classical vectors, the Hamiltonian in Eq. (5) can be solved numerically. I rescaled the energies by the exchange constant J to bring the system into natural units. The final Hamiltonian of clock anisotropy to solve is, in natural units,

$$\begin{aligned}\hat{\mathcal{H}} &= 2\hat{\mathbf{S_1}}\cdot\hat{\mathbf{S_2}} \\ &+ E_A(\cos 6\theta_1 + \cos 6\theta_2) \\ &- E_Z\hat{\mathbf{B}}\cdot(\hat{\mathbf{S_1}} + \hat{\mathbf{S_2}})\end{aligned} \tag{6}$$

where $\hat{\mathbf{S_1}}, \hat{\mathbf{S_2}}, \hat{\mathbf{B}}$ are all unit vectors in the directions of $\vec{S_1}, \vec{S_2}, \vec{B}$ respectively. And using a unitless parameter for the Zeeman energy proportional to the magnetic field strength

$$E_Z \equiv \frac{g_\perp \mu_B |\vec{B}|}{J} \tag{7}$$

This clock-anisotropy model is compared throughout with a uniaxial model with an anisotropy term $E_A(\cos(2\theta_1) + \cos(2\theta_2))$. These models can both be written as a generalised axial anisotropy Hamiltonian

$$\begin{aligned}\hat{\mathcal{H}}(\theta_1,\theta_2) &= 2\cos(\theta_1 - \theta_2) \\ &+ E_A(\cos n\theta_1 + \cos n\theta_2) \\ &- E_Z(\cos(\theta_1 - \theta_B) + \cos(\theta_2 - \theta_B))\end{aligned} \tag{8}$$

where $\theta_1, \theta_2, \theta_B$ are the azimuth of $\hat{S_1}, \hat{S_2}, \hat{B}$ respectively and $n = 2$ for the uniaxial case, $n = 6$ for the clock-type case.

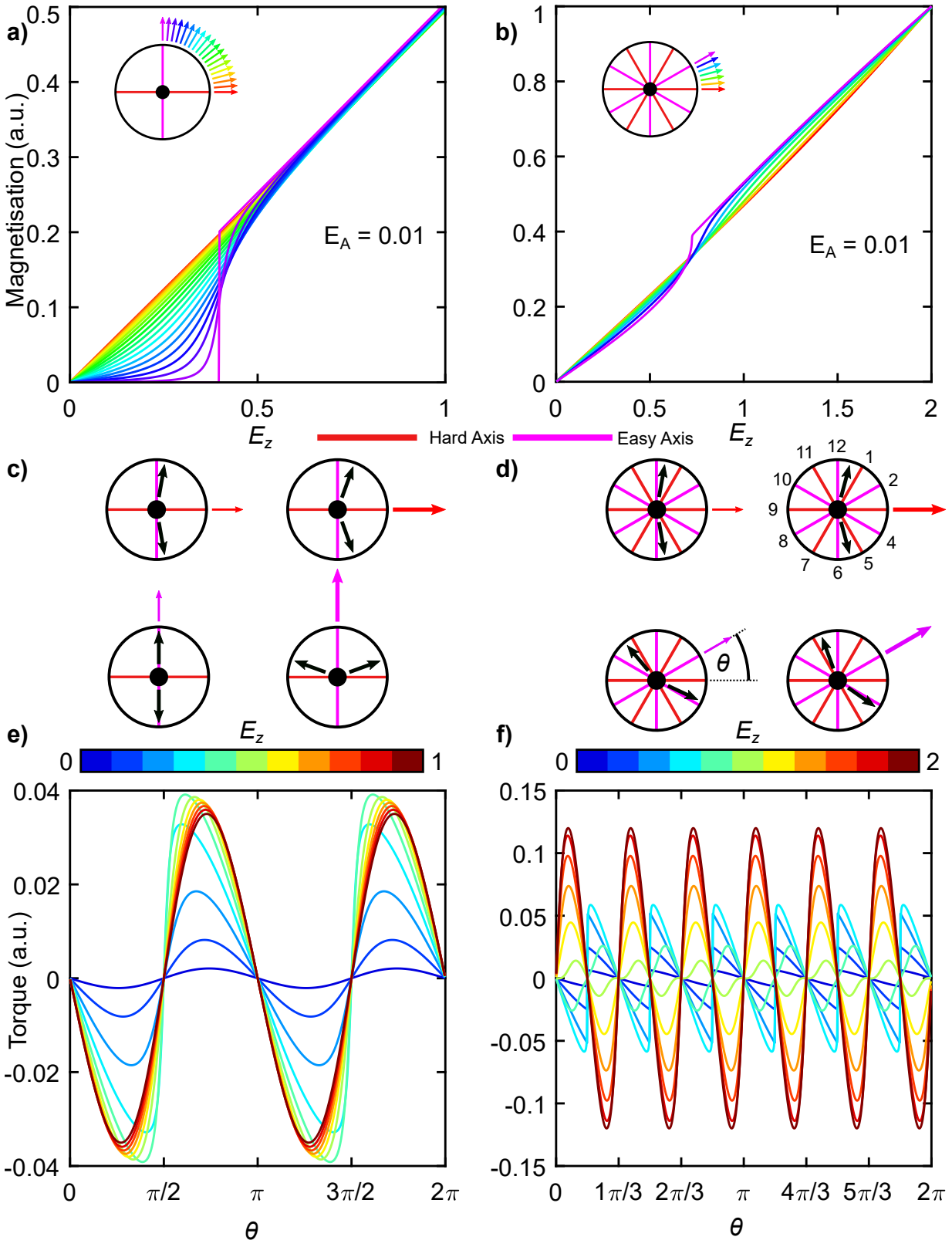

FIG. 2. **Mean field calculations of the two-sublattice model** From top to bottom: magnetisation curves, equilibrium spin orientation as function of applied field strength, magnetic torque as function of field orientation for fixed field strength for uniaxial (left column) and clock-type (right column) anisotropy in Eq. (8). In a), b) colour indicates field orientation, see inset. In c), d) top (bottom) row indicates field applied along hard (easy) axis. For clock anisotropy the behavior is shown for the magnetic domain with the lowest energy. θ is measured from the hard axis,

This comparison is useful because the uniaxial system is well understood [19–21] so it is informative to compare analogous properties between the two systems.

To solve this system numerically I minimise the value of H with gradient descent. Finding the global minimum by using starting points on each of the solutions to the case where there is zero applied field. However, it needs to be noted that in this problem, as stated is an almost pathological example for gradient descent. This is because with the coordinate transform $x = \frac{1}{2}(\theta_1 - \theta_2), y = \frac{1}{2}(\theta_1 + \theta_2)$ the Hamiltonian becomes

$$\begin{aligned}\hat{\mathcal{H}}(x,y) &= 2\cos 2x \\ &+ 2E_A \cos nx \cos ny \\ &- 2E_Z \cos(y - \theta_B)\cos x\end{aligned} \tag{9}$$

which is only weakly dependent on y when $E_A, E_Z \ll 1$. This problem can be solved using an approximate preconditioning matrix [22], which performs a coordinate transform to bring the system into a more well-conditioned form. The numerical system is a perfectly parallel problem and so it can be solved quickly on a small cluster or large server CPU. The code to solve this was written in C++ to maximise speed, especially in parallelisation. This was run on two Intel Xeon E5-2650 CPUs on a Linux server, across all 32 cores. In this set up it can solve 1 million points in 6 s. This enabled me to solve it at high resolution for a large range of parameters; the final dataset, containing 2^{29} points, was completed in under 90 min. To show qualitative effects of the anisotropy, large values of E_A are shown in Figure 2, however quantitative analysis was also performed. This strategy of finding the global minimum means that only the magnetic domain with the lowest energy is considered.

Numerical Results

Figure 2 shows the results of the calculations comparing the uniaxial and the clock-type cases using Eq. (8). Figure 2a,b shows the evolution of magnetisation projected onto the magnetic field direction $(\vec{S_1} + \vec{S_2}) \cdot \hat{\mathbf{B}}$ with field strength for $E_A = 0.01$ in 5° increments in the field orientation with respect to the hard axis. In the uniaxial case (a), a clear spin-flop can be seen with a discontinuity in magnetisation when the field is parallel to the easy axis. The field at which this occurs is quadratic with E_A when $E_A \ll 1$,

$$E_{Z(SF)} = 4\sqrt{E_A - E_A^2} \tag{10}$$

but as there is a discontinuity it is a clear experimental signature of anisotropy. For fields angled away from the easy axis the change in magnetisation is more gradual, with no clear transition between low and high fields. Note: in these units, a magnetisation of 2 means the magnetisation is fully saturated along the field direction.

For the clock-anisotropy case (Figure 2b), with field applied along the easy axis and selecting the domain with the lowest energy, there is a small anomaly in magnetisation (magenta curve). This quickly changes to a smooth crossover as the field is tilted away from the easy axis. For very strong anisotropy $E_A \gtrapprox 0.015$ (not shown) there is also a discontinuity is magnetisation which occurs at $\approx 2\times$ higher field.

The qualitative effect of the spin-reorientations as a function of applied field in the clock-anisotropy crystal can be seen in Figure 2d. The axes are numbered as on a clock. With field application along an easy axis #4, the spin start antiparallel close to #2 and #8. There is a non-zero susceptibility as the spins can both tilt towards the field. This reduces the energy from the Zeeman term and provides a non-zero magnetisation. At a special field value, one of the spins moves over a hard axis (#7), leading to an anomaly in magnetisation. It should be noted that above $E_Z \gtrapprox 4$ a second anomaly would be expected in this arrangement. This will occur when both spins move over the next hard axis such that the spins are both close to #4 and the magnetisation is nearly saturated. However, this high field regime is not considered here, as it would require experimentally inaccessible fields. This magnetic transition is very different to the uniaxial case, seen in Figure 2c. For field applications parallel to the easy axis (Figure 2c, bottom row), at low fields the spins are parallel and antiparallel with the field. The spins cannot rotate towards the field to reduce their energy and so there is zero susceptibility. At the spin flop, it becomes energetically favorable to move the spins into the arrangement shown, where they can lower their energy by rotating towards the field.

An experimental approach that is a sensitive probe measuring anisotropy is torque magnetometry [23–26]. This measures the magnetic torque on a sample which is defined as

$$\tau = \vec{m} \times \vec{B} \tag{11}$$

and can be written in terms of the free energy

$$\tau \cdot \hat{\mathbf{v}} = -\frac{\partial F}{\partial \theta_v} \tag{12}$$

where θ_v is the rotation of the sample (or equivalently the field) about the axis $\vec{v}$. Thus, magnetic torque is the tendency for the system to minimise its magnetic energy by changing its orientation. As can be seen in Eq. (12), it is sensitive only to the anisotropic part of of the magnetisation. In an isotropic system, the free energy F cannot depend on sample orientation and so the torque must be 0. As is discussed in [26], in a uniaxial system, in the low field limit, the torque can be found analytically to be proportional to the difference in susceptibility between the easy axis and the hard axis

$$\tau = \frac{1}{2\mu_0}(\chi_\perp - \chi_\parallel)B^2 \sin 2\theta \tag{13}$$

As torque is measured while rotating the sample, different kinds of anisotropy could be differentiated by the periodicity of the torque signal. In this system, free energy varies with field orientation (Figure SM1), so the crystal will experience a magnetic torque to minimise the free energy. For example,

Figure 2e shows the magnetic torque produced from a uniaxial crystal for a range of field strengths. The crystal orientation with field parallel to a hard axis has spin arrangement with both spins on an easy axis, and able to reduce their Zeeman energy. This is a lower energy state than the orientation with field parallel to the easy axis. The torque signal is not sinusoidal as it would be in an anisotropic paramagnet, it is steeper when the field passes through the easy axis. This can provide a clear mark of which axis is which if the field is in the range of the spin-flop field. The torque from the clock-type case (Figure 2f) is much more complex. At low fields, it appears similar to the uniaxial case, but has sixfold symmetry. However the sign of the torque changes when E_Z passes ≈ 1. This is independent of the magnitude of E_A.

These results provide guidance to design an experiment to determine the magnetic properties of a crystal sample. A magnetisation experiment as a function of magnetic field could show the presence of a spin flop. The location of the spin flop in E_Z, and the size of the jump in magnetisation can be used to determine E_A. A second experimental probe, magnetic torque, can clearly show the difference between uniaxial and clock type systems. Quantitatively E_A may however be determined by finding the magnitude of the torque signal in absolute units and comparing to calculation.

VIBRATING SAMPLE MAGNETOMETRY

Principle of operation

A vibrating-sample magnetometer (VSM) is able to detect the magnetisation of a sample by vibrating it in an inductive coil and measuring the voltage pickup as shown in Figure 3a. From Lenz' law, the inductive voltage in the coil is

$$V = -\frac{\partial \Phi}{\partial t} \tag{14}$$

$$= -\frac{\partial \Phi}{\partial z}\frac{\partial z}{\partial t} \tag{15}$$

By approximating the sample as a point dipole, and using $z = A\cos(\omega t)$, the pickup voltage can be approximated.

$$V = A\omega C|\vec{m}|\sin(\omega t) \tag{16}$$

with vibration amplitude A, vibration frequency ω, coupling constant C, and magnetic dipole moment $\vec{m}$ [27].

By measuring this inductive voltage, the magnetic dipole moment of a mounted sample can be measured precisely. The experiment is performed in a PPMS (Physical Property Measurement System) that controls temperature down to 3 K and magnetic field of the sample up to 16 T.

Methods

A $CoTiO_3$ crystal was aligned with x-ray diffraction and had faces cut perpendicular to crystal axes $\vec{a^*}$, $\vec{b}$, $\vec{c}$ to allow for alignment when mounting. This cut crystal, weighing 46.0 mg, was mounted on in the VSM assembly such that the applied field would be parallel to the $\vec{a^*}$ axis (Figure 3b. A VSM experiment was performed measuring the magnetic moment on cooling from 300 K to 5 K with an applied field of 0.1 T. A second measurement recorded the magnetic moment in a field hysteresis between -16 T and 16 T at temperatures between 5 K, and 40 K. This experiment was repeated with the crystal rotated 90°, such that the field was parallel to $\vec{b}$ (Figure 3a). The experiment was also performed on a second cut crystal, weighing 11.2 mg, with the magnetic field applied along the $\vec{c}$ axis. All VSM measurements were performed with a 40 Hz, 1 mm oscillation.

Results

Figure 3 shows the results of the VSM experiment. Figure 3b shows the evolution of the magnetisation of the sample with temperature for different crystal orientations. The curves for the fields along $\vec{a^*}$ and $\vec{b}$ lie on top of each other to within the error of the experiment. By fitting the susceptibility per spin data to a Curie Weiss relationship [28]

$$\chi = \chi_0 + \frac{\mu_{eff}^2}{3\mu_0 k_B (T + \theta_W)} \quad \text{(per spin)} \tag{17}$$

I can extract the effective magnetic moment of the spins μ_{eff}, and the Weiss temperature θ_W as shown in Table I. For all orientations, the Weiss temperature T_W differs from the Néel temperature (T_N) of 38 K, suggesting that $CoTiO_3$ is not a conventional antiferromagnet.

TABLE I. Extracted parameters from Curie-Weiss fit to magnetic susceptibility for different orientations.

	μ_{eff} (μ_B)	θ_W (K)	χ_0 (μ_BT^{-1})
$\vec{B} \parallel \vec{a^*}$	4.71	11.0	0.011
$\vec{B} \parallel \vec{b}$	4.76	9.6	0.010
$\vec{B} \parallel \vec{c}$	2.12	28.0	0.008

The anisotropy in μ_{eff} between the ab plane and the $\vec{c}$ axis is caused by an anisotropic g factor (eq 3). This means that spins get less Zeeman energy from tilting towards the $\vec{c}$ axis than towards a vector in the ab plane. As such, there is a lower susceptibility for fields parallel to $\vec{c}$.

Figure 3c,d show the evolution of magnetisation with applied magnetic field. For fields applied parallel to $\vec{a^*}$, and $\vec{b}$, the two curves follow each other very closely and no spin-flop transition can be seen. This could occur if the spin-flop was sufficiently weak that it cannot be captured by this experiment (suggesting that E_A is small). Alternatively, if the easy and hard axes are rotated approximately 15° from the crystal axes it would put $\vec{a^*}$ and $\vec{b}$ in-between the easy and hard axes of the anisotropy. If this were the case one would expect the two curves to follow each other. There is also a clear anomaly in

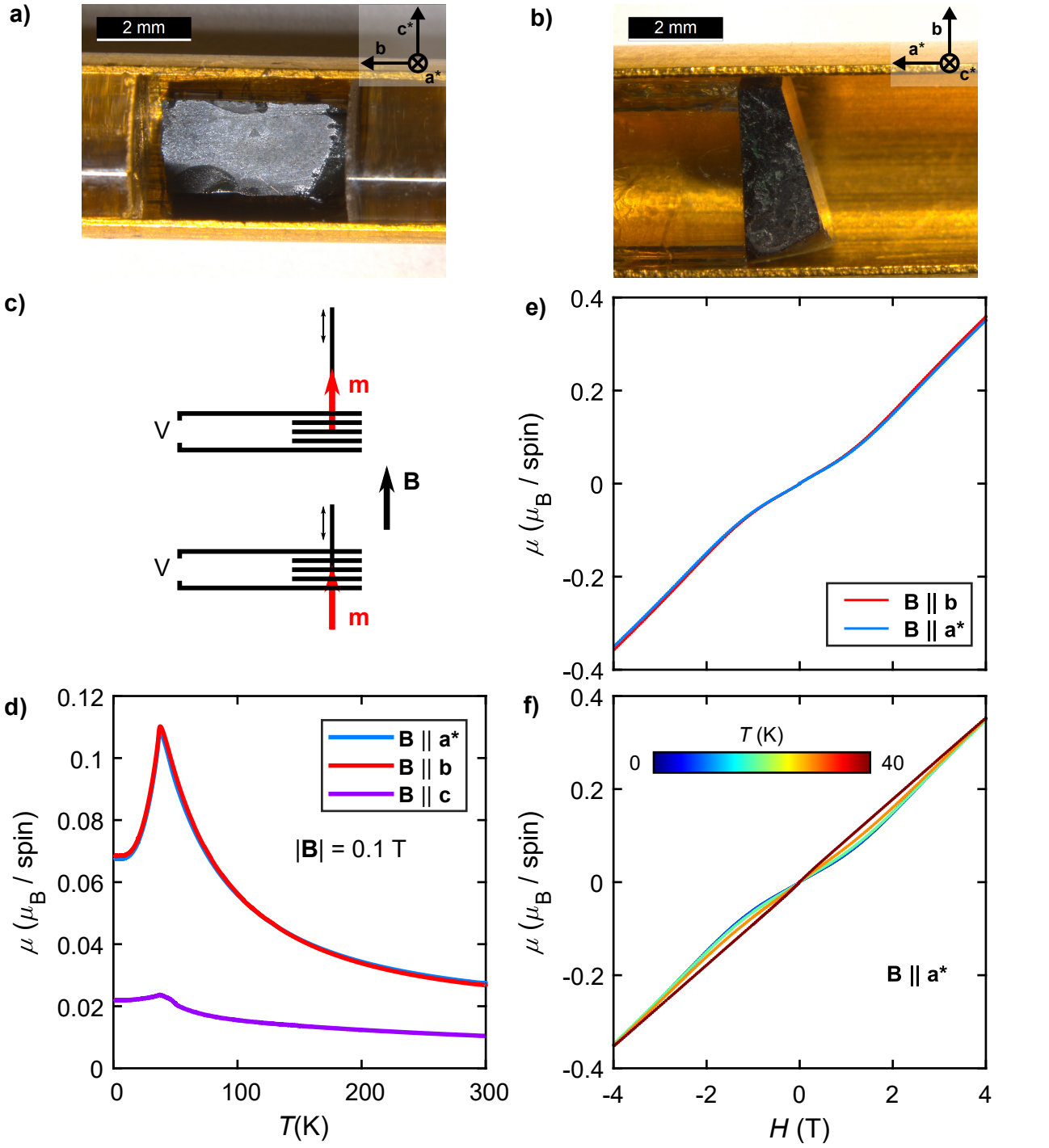

FIG. 3. **Vibrating Sample Magnetometry** Microscope photograph of mounted $CoTiO_3$ crystal for VSM experiment with magnetic field applied (a) $\vec{B} \parallel \vec{b}$ and (b) $\vec{B} \parallel \vec{a^*}$. (c) Schematic showing motion of sample in inductive coil at two different time steps. (d) Evolution of sample magnetisation with temperature for different sample orientations. Evolution of sample magnetisation with applied field for (e) different sample orientations and (f) a range of temperatures from 3 K to 40 K.

the region between -1 T to 1 T. The evolution of magnetisation with magnetic field for different temperatures from 5 K to 40 K can be seen in Figure 3d. This shows the anomaly developing as the temperature drops below the Néel temperature. The anomaly is not present in magnetisation curves for $\vec{B} \parallel \vec{c}$ (Figure SM2). This magnetisation study provided significant information about the system, but was unable to identify the characteristic features of clock anisotropy. This is because, as can be seen in Figure 2b clock anisotropy has particularly weak spin-flop features.

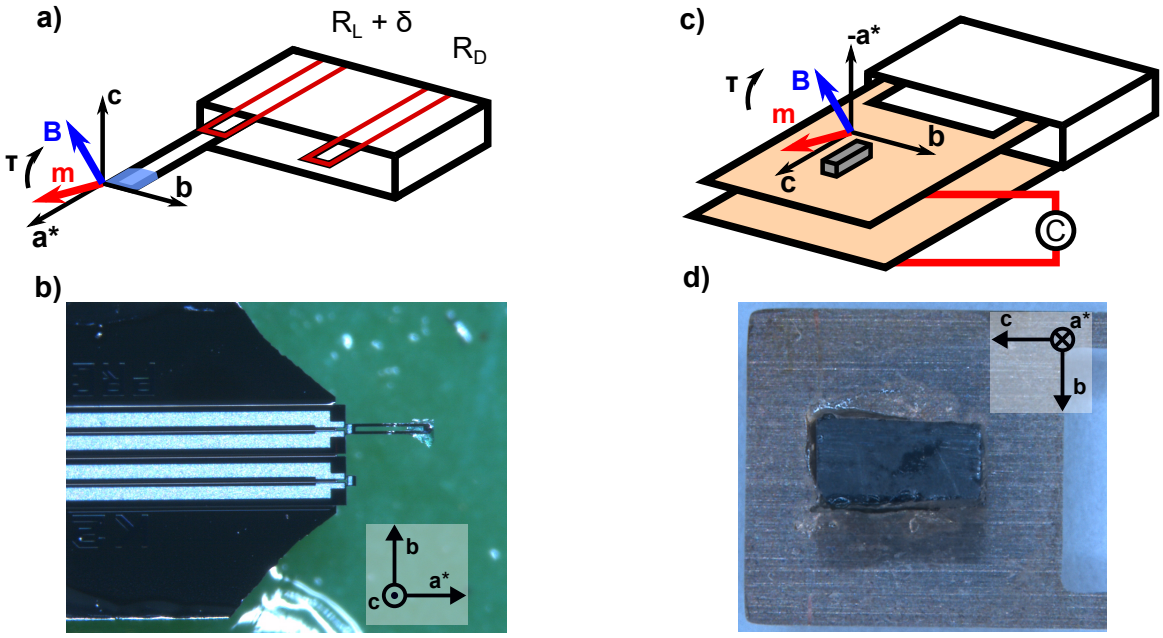

FIG. 4. **Torque Magnetometer designs** (a) Schematic showing layout of piezoresistive cantilever. b. Microscope image of mounted $CoTiO_3$ crystal on cantilever. (c) Schematic showing layout of capacitive cantilever. d. Microscope of mounted $CoTiO_3$ crystal on capacitive cantilever.

TORQUE MAGNETOMETRY

Principle of operation

Torque magnetometry generally involves mounting the sample on a long cantilever and placing the assembly in a magnetic field. Various methods can be used to measure the deflection of the lever. One method uses a piezoresistive lever [29]. As the lever deflects, the mechanical strain at the base increases its resistance. This resistance is measured by having a current path through the lever be one part of a Wheatstone bridge as shown in Figure 4a. A second method measures the capacitance between the lever and a nearby plate, shown in Figure 4c.

Preliminary results

A first experiment using a $400\,\mu m$ Seiko PRC400 piezoresistive cantilever torque magnetometer has been performed. To prepare samples, small crystals were flaked off the larger piece of $CoTiO_3$. Of the pieces that appeared under the microscope to be single, flat crystals of approximately $100\,\mu m$ wide, were tested with x-ray diffraction. From these, samples were selected with a surface normal parallel to one of the crystal axes.

A sample S1 with a surface normal parallel to the $\vec{c}$ axis was mounted on the lever and stuck with grease. The torque was measured in in the $\vec{a^*}$, $\vec{c}$ plane. The torque signal was fitted to a sinusoidal form

$$\tau = A \sin 2(\theta - \theta_0) + B \tag{18}$$

with free parameters A, B, and θ_0, from Eq. (13). The evolution of the amplitude A of the torque signal with temperature is shown in Figure 5. The data clearly show the transition of the sample from a paramagnetic state above the Néel temperature to an antiferromagnetic state below it. These data match with those gathered during the VSM experiment (Figure 3d).

A second sample S2 with a surface normal parallel to the $\vec{b}$ axis was mounted on another identical lever. The evolution of the torque signal with temperature can be seen in Figure 5d. Above the Néel temperature, some paramagnetic torque signal is present which matches the torque in ac, caused by the crystal being tilted slightly, such that some ac component remains. The sign of this high temperature signal is reversed from the previous data because the lever is oriented in the opposite direction. Below the transition, a more complex torque profile can be seen. This profile has 2-fold symmetry, and peaks separated approximately $90°$ apart. By assuming the contribution from the ac plane is constant below $50\,K$ I subtract this component, leaving only the in-plane contribution (Figure 5d. This shows signs of in-plane structure. The evolution of this signal with field at $3\,K$ can be seen in Figure SM3. These data show that above $4\,T$, a sinusoidal pattern of torque is recovered. This clearly shows that the field is tilted towards $\vec{c}$, and so the expected torque is beyond the scope of the calculation. Including that contribution would require a generalisation of the model to include three-dimensional field orientations, anisotropic g-factors, and a component from the exchange interactions to hold the spins in the ab plane.

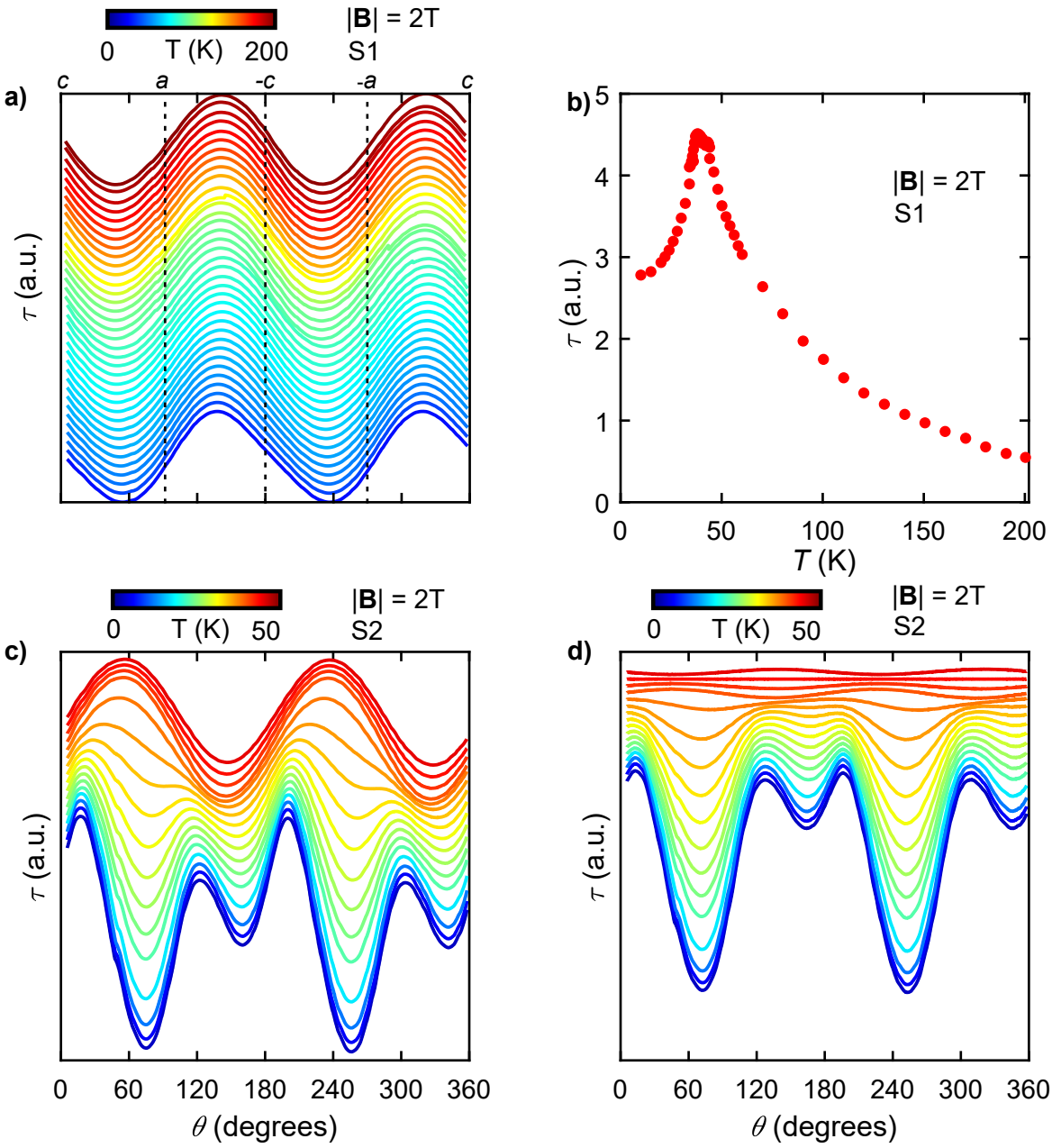

FIG. 5. a) Evolution of torque on $CoTiO_3$ with crystal rotation about axis $\vec{b}$ for a range of temperatures between 5 K and 200 K at 2 T. b) Evolution of fitted amplitude of torque signal on $CoTiO_3$ with temperature at 2 T. Evolution of torque on $CoTiO_3$ with crystal rotation about axis $\vec{c}$ for a range of temperatures between 5 K and 50 K at 2 T as (c) raw data, and (d) with high temperature data subtracted.

OTHER WORK

During this year, I wrote the first draft of a paper of which I am the first author. This work was on an ARPES study of the superconductor $FeSe_{0.82}S_{0.18}$ which started during my MPhys project. The work will be submitted this year after further improvements [30]. I have found the process of writing a paper has significantly improved my experimental planning skills, as I now have more experience in what problems can come up during this work.

FUTURE WORK

A number of improvements could be make to the clock-anisotropy calculation. The assumption that the spins are bounded to the ab plane relies on the crystal being perfectly aligned. This assumption could be relaxed by considering the state of any crystal orientation. The calculation could be generalised by allowing the sublattice spins to move out of the ab plane and computing the state for magnetic fields on a sphere. This could be implemented practically by mapping the mag-

netic field direction onto a Fibonacci spiral, distributed over a sphere [31]. This strategy is well developed for computer graphics and has very good area coverage of the unit sphere when many points are considered. In order to manage the complexity of the additional dimensionality, the code could be modified to execute on a graphics card for significant speedup. This would allow the theoretical model to be generalised with anisotropic g factors, and an energy component to hold the spins within the ab plane. This would allow the calculation to include the effect of field orientation titled towards $\vec{c}$ and might capture the complex behavior observed. Additionally, the effects of magnetic domains could be considered by treating all domains separately, allowing the effects of domain polarisation to be included.

One challenge of the present experiments is to accurately align the samples to probe the anisotropy in the ab plane while suppressing contributions from the out of plane tilt. A way forward may be to implement in-situ rotations of the torque lever using a multi-axis rotator such as the recently purchased Attocube micro-goniometers. This project would help widely with a range of projects where precision alignment is necessary as the system is sensitive to sample orientation, or where in-situ rotation could be useful. I am also planning additional torque magnetometry experiments with the Materials Science department using a capacitive lever. This allows much larger samples to be mounted which could allow more precise alignment of the crystal. I also plan to explore other magnetic systems with torque magnetometry such as single crystals of insulating triangular lattice based Yb magnet $Ba_3Yb(BO_3)_3$, recently synthesised in our research group. This is a candidate material to display bond-dependent interactions between an effective spin-$\frac{1}{2}$ Yb ions on a triangular lattice, characterised so far my magnetisation and temperature-dependent susceptibility measurements.

Another area that I am planning to be involved in is in neutron scattering experiments, on $CoTiO_3$ and in other, related, materials. These include frustrated magnetic systems, quantum magnets. Neutron scattering to explore the magnon band structure provides an incredible amount of detail about the magnetic Hamiltonian of a system. This could be combined with other magnetometry experiments like the ones above, and similar calculations and toy models to test aspects of the predicted Hamiltonians. Finally, I am planning to be involved in future heat capacity studies performed in a dilution refrigerator that is currently being set up in a new lab. This would open up many more properties of these materials for study.

[1] A. H. Castro Neto, F. Guinea, N. M. R. Peres, K. S. Novoselov, and A. K. Geim, The electronic properties of graphene, RvMP **81**, 109 (2009).

[2] F. D. M. Haldane, Nobel lecture: Topological quantum matter, Reviews of Modern Physics **89**, 040502 (2017).

[3] M. Z. Hasan and C. L. Kane, Colloquium: topological insulators, Reviews of modern physics **82**, 3045 (2010).

[4] Y. Cao, V. Fatemi, S. Fang, K. Watanabe, T. Taniguchi, E. Kaxiras, and P. Jarillo-Herrero, Unconventional superconductivity in magic-angle graphene superlattices, Nature **556**, 43 (2018).

[5] B. Yan and C. Felser, Topological materials: Weyl semimetals, Annual Review of Condensed Matter Physics **8**, 337 (2017).

[6] R. Shindou, R. Matsumoto, S. Murakami, and J.-i. Ohe, Topological chiral magnonic edge mode in a magnonic crystal, Physical Review B **87**, 174427 (2013).

[7] A. Mook, J. Henk, and I. Mertig, Tunable magnon weyl points in ferromagnetic pyrochlores, Physical review letters **117**, 157204 (2016).

[8] S. S. Pershoguba, S. Banerjee, J. Lashley, J. Park, H. Ågren, G. Aeppli, and A. V. Balatsky, Dirac magnons in honeycomb ferromagnets, Physical Review X **8**, 011010 (2018).

[9] F. Schwierz, Graphene transistors, Nature nanotechnology **5**, 487 (2010).

[10] A. Grigorenko, M. Polini, and K. Novoselov, Graphene plasmonics, Nature photonics **6**, 749 (2012).

[11] X. Huang, X. Qi, F. Boey, and H. Zhang, Graphene-based composites, Chemical Society Reviews **41**, 666 (2012).

[12] M. Elliot, P. McClarty, D. Prabhakaran, R. Johnson, H. Walker, P. Manuel, and R. Coldea, Visualization of isospin momentum texture of dirac magnons and excitons in a honeycomb quantum magnet, arXiv preprint arXiv:2007.04199 (2020).

[13] B. Yuan, I. Khait, G.-J. Shu, F. Chou, M. Stone, J. Clancy, A. Paramekanti, and Y.-J. Kim, Dirac magnons in a honeycomb lattice quantum xy magnet cotio 3, Physical Review X **10**, 011062 (2020).

[14] R. Newnham, J. Fang, and R. Santoro, Crystal structure and magnetic properties of cotio3, Acta Crystallographica **17**, 240 (1964).

[15] J. Villain, R. Bidaux, J.-P. Carton, and R. Conte, Order as an effect of disorder, Journal de Physique **41**, 1263 (1980).

[16] C. L. Henley, Ordering due to disorder in a frustrated vector antiferromagnet, Physical review letters **62**, 2056 (1989).

[17] R. Moessner and J. T. Chalker, Low-temperature properties of classical geometrically frustrated antiferromagnets, Physical Review B **58**, 12049 (1998).

[18] A. V. Chubukov and T. Jolicoeur, Order-from-disorder phenomena in heisenberg antiferromagnets on a triangular lattice, Physical review B **46**, 11137 (1992).

[19] A. Bogdanov, A. Zhuravlev, and U. Rößler, Spin-flop transition in uniaxial antiferromagnets: Magnetic phases, reorientation effects, and multidomain states, Physical Review B **75**, 094425 (2007).

[20] N. Yamashita, Field induced phase transitions in uniaxial antiferromagnets, Journal of the Physical Society of Japan **32**, 610 (1972).

[21] H. Rohrer and H. Thomas, Phase transitions in the uniaxial antiferromagnet, Journal of Applied Physics **40**, 1025 (1969).

[22] A. V. Knyazev, Preconditioned eigensolvers—an oxymoron, Electron. Trans. Numer. Anal **7**, 104 (1998).

[23] H. Williams, Some uses of the torque magnetometer, Review of Scientific Instruments **8**, 56 (1937).

[24] A. Cornia, D. Gatteschi, and R. Sessoli, New experimental techniques for magnetic anisotropy in molecular materials, Coordination Chemistry Reviews **219**, 573 (2001).

[25] B. Matthaei, J. Franse, S. Sinnema, and R. Radwński, Torque measurements on single-crystalline y2co17, gd2co17 and y2fe17, Le Journal de Physique Colloques **49**, C8 (1988).

[26] U. Gäfvert, L. Lundgren, B. Westerstrandh, and O. Beckman, Crystalline anisotropy energy of uniaxial antiferromagnets evaluated from low field torque data, Journal of Physics and Chemistry of Solids **38**, 1333 (1977).

[27] Q. Design, *VSM Option User's Manual* (2011).
[28] S. Blundell, *Magnetism in condensed matter* (Oxford University Press, 2003).
[29] C. Rossel, P. Bauer, D. Zech, J. Hofer, M. Willemin, and H. Keller, Active microlevers as miniature torque magnetometers, Journal of applied physics **79**, 8166 (1996).
[30] K. MacFarquharson, P. Reiss, A. A. Haghighirad, T. K. Kim, and A. I. Coldea, Revealing the coexistence of the bulk and surface electronic states by in-situ K dosing in the tetragonal superconductor $FeSe_{0.82}S_{0.18}$, (In preparation) (2020).
[31] D. P. Hardin, T. Michaels, and E. B. Saff, A comparison of popular point configurations on $\mathbb{S}^2$, arXiv preprint arXiv:1607.04590 (2016).

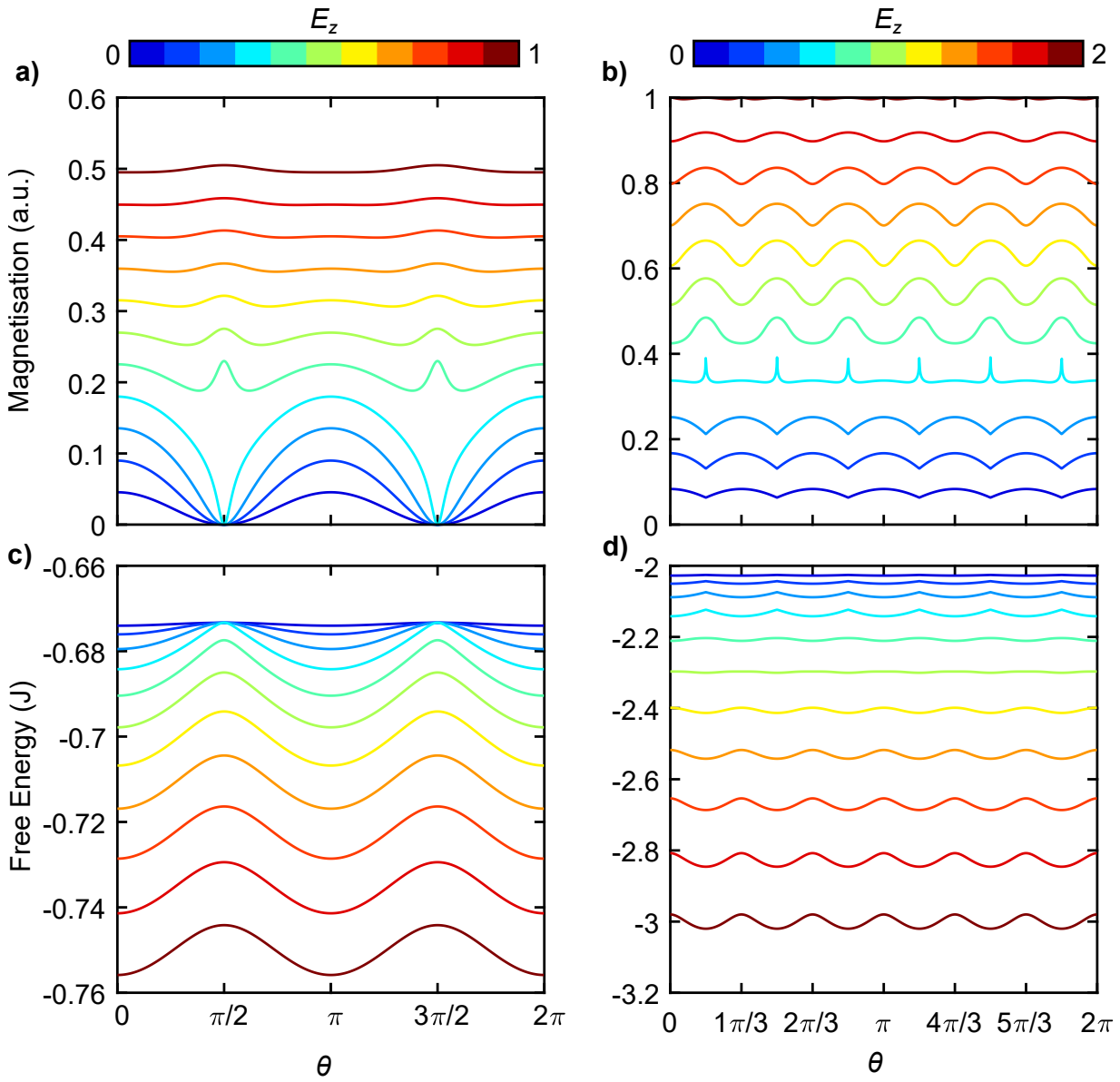

FIG. SM1. **Supplementary Materials for mean field calculations of the two-sublattice model** From top to bottom: magnetisation as a function of field orientation for fixed field strength, equilibrium energy as a function of field orientation for fixed field strength for uniaxial (left column) and clock-type (right column) anisotropy. For clock anisotropy the behavior is shown for the magnetic domain with the lowest energy.

SUPPLEMENTARY MATERIALS

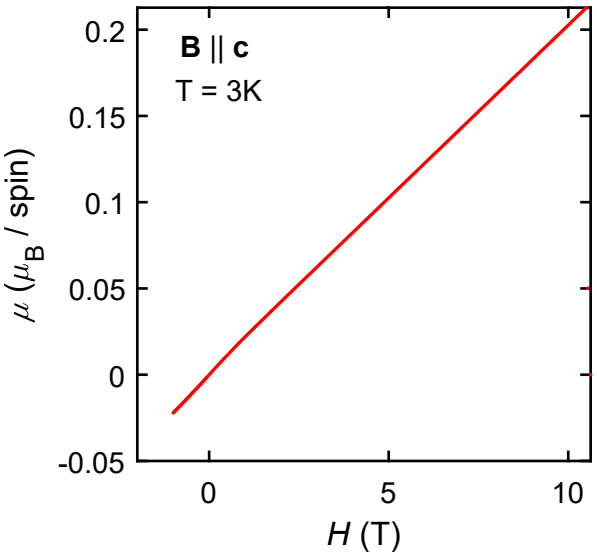

FIG. SM2. Evolution of $CoTiO_3$ sample magnetisation with applied field for field parallel to the $\vec{c}$ axis at 3 K

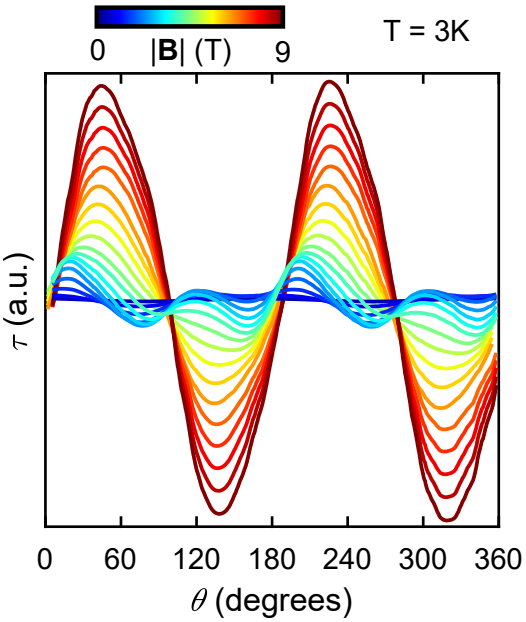

FIG. SM3. Evolution of torque on $CoTiO_3$ with crystal rotation about axis $\vec{c}$ for a range of fields from $0.5\,\mathrm{T}$ to $9.0\,\mathrm{T}$ at $3\,\mathrm{K}$.